AD-A118 836 SCIENCE APPLICATIONS INC MCLEAN VA F/G 4/2
NUMERICAL MODELING OF TROPICAL WEATHER SYSTEMS.(U)
AUG 82 S CHANG N00014-81-C-2224
UNCLASSIFIED NL

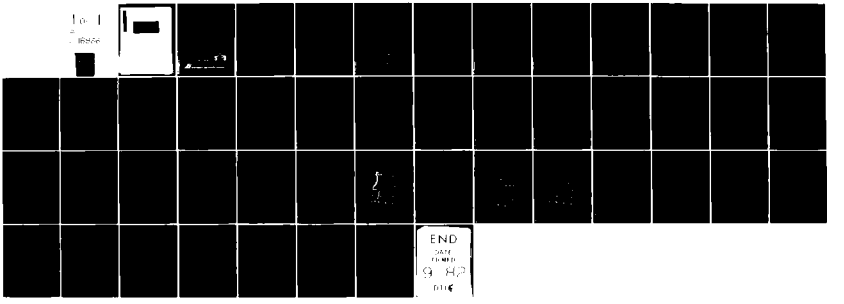

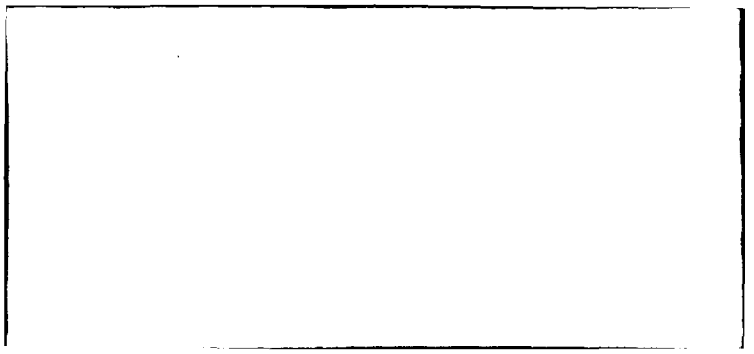

(12)

# NUMERICAL MODELING OF TROPICAL WEATHER SYSTEMS

FINAL REPORT

SAI-83-895-WA





SAI
ATLANTA • [illegible] • [illegible] • [illegible] • [illegible] • [illegible] • [illegible] • LA JOLLA
[illegible] • [illegible] • [illegible] • [illegible] • [illegible] • [illegible]

# NUMERICAL MODELING OF TROPICAL WEATHER SYSTEMS

FINAL REPORT

SAI-83-895-WA

Submitted to:

Environmental Sciences Division
Naval Research Laboratory
Washington, D.C. 20375

Prepared Under:

Contract No. N00014-81-C-2224
SAI Project No. 1-157-18-351-00

Prepared by:

Simon Chang

August 1982

SCIENCE APPLICATIONS, INC.
1710 Goodridge Drive, McLean, VA 22102
(703) 734-5840

SECURITY CLASSIFICATION OF THIS PAGE (When Data Entered)

| REPORT DOCUMENTATION PAGE | READ INSTRUCTIONS BEFORE COMPLETING FORM |
|---|---|
| 1. REPORT NUMBER | 2. GOVT ACCESSION NO. AD-A118836 | 3. RECIPIENT'S CATALOG NUMBER |
| 4. TITLE (and Subtitle) Numerical Modeling of Tropical Weather Systems | 5. TYPE OF REPORT & PERIOD COVERED Final Report 15 Apr 81 - 12 Jun 82 |
| | 6. PERFORMING ORG. REPORT NUMBER |
| 7. AUTHOR(s) Simon Chang | 8. CONTRACT OR GRANT NUMBER(s) N00014-81-C-2224 |
| 9. PERFORMING ORGANIZATION NAME AND ADDRESS Science Applications, Inc. 1710 Goodridge Dr. McLean, Va. 22102 | 10. PROGRAM ELEMENT, PROJECT, TASK AREA & WORK UNIT NUMBERS |
| 11. CONTROLLING OFFICE NAME AND ADDRESS Naval Research Laboratory 4555 Overlook Avenue, S.W. Washington, D.C. 20375 | 12. REPORT DATE August 1982 |
| | 13. NUMBER OF PAGES |
| 14. MONITORING AGENCY NAME & ADDRESS(if different from Controlling Office) | 15. SECURITY CLASS. (of this report) Unclassified |
| | 15a. DECLASSIFICATION/DOWNGRADING SCHEDULE |

16. DISTRIBUTION STATEMENT (of this Report)

DISTRIBUTION STATEMENT A
Approved for public release;
Distribution Unlimited

17. DISTRIBUTION STATEMENT (of the abstract entered in Block 20, if different from Report)

18. SUPPLEMENTARY NOTES

19. KEY WORDS (Continue on reverse side if necessary and identify by block number)

Tropical weather systems, numerical weather prediction, monsoon depression, tropical cyclone, easterly wave.

20. ABSTRACT (Continue on reverse side if necessary and identify by block number)

This final report documents the efforts on numerical simulations of tropical weather systems. Tropical weather systems investigated include the Indian Ocean monsoon depressions, tropical cyclones, and easterly waves.

DD FORM 1 JAN 73 1473 EDITION OF 1 NOV 65 IS OBSOLETE
S/N 0102-LF-014-6601

SECURITY CLASSIFICATION OF THIS PAGE (When Data Entered)

For the numerical simulation of Indian Ocean monsoon depression, an idealized zonal current pertinent to summer monsoon conditions is used as the basic flow. Initial perturbations superposed on the basic flow consist of a prescribed heating source. The simulated winds at 48 and 72 h are discussed. The simulation reproduces many observed phenomena, including the storm track. But the cumulus parameterization currently used in the NRL mesoscale model yields unrealistically heavy rainfall on steep mountain slopes. It needs modification in future use.

Numerical simulation is also carried out to simulate the interaction of two tropical cyclones (Fujiwhara effects). Results show that on an f-plane with no mean wind, the movements of the two cyclones consist of a mutual cyclonic rotation, mutual attraction, and eventual coalescense. The trajectories of two tropical cyclones of equal (different) strength are symmetric (asymmetric) relative to the center of mass of the two storms. Further numerical experiments indicate that the latitudinal variation of the Coriolis parameter has great influence on the trajectories.

Concerning easterly waves, we attempted to simulate the transformation of an easterly wave into an incipient tropical depression. In a uniform easterly current, the NRL mesoscale model successfully simulates the formation of an easterly wave. It has very realistic latitudinal components and relative humidity field, but the upward motion in the trough is too strong. We suggest for future study latitudinal shear in the mean current and variation of the Coriolis parameter be included in the model.

TABLE OF CONTENTS

# CHAPTER 1. INTRODUCTION

This final technical report documents the research efforts in the numerical simulation of tropical weather systems carried out under the auspices of ONR Contract N00014-81-C-2224, for the Atmospheric Physics Branch, Environmental Sciences Division, of the Naval Research Laboratory (NRL).

The research efforts can be topically separated into three areas; namely, monsoon depressions, interactions of typhoon pairs, and easterly waves. In the following three chapters, we will discuss in detail the research efforts and results obtained in each of these areas. In short, the following tasks have been completed:

(1) A dynamic initialization scheme through prescribed heating was devised so that dynamically consistent tropical disturbances including the convergence component can be realistically simulated in the NRL mesoscale model.

(2) Major modifications of the NRL mesoscale model were carried out to facilitate simulation studies of tropical weather systems. The modifications include changes in grid system structure, spatial resolution, cyclic boundary conditions, and incorporation of topography.

(3) Realistic simulations of easterly waves and monsoon depressions have been accomplished. Problem areas for future research have been identified and solutions are suggested.

In addition, all computer codes generated in connection with our efforts have been transferred to Naval Research Laboratory personnel and are stored in the TI-ASC in both softcopy and hardcopy forms. Some of these codes can be implemented in the Navy's operational forecasting models to improve weather forecasting in a number of tropical regions.

# CHAPTER 2. MONSOON DEPRESSION

## 2.1 BACKGROUND

The summer and winter monsoons of south Asia constitute very pronounced regional anomalies in the general circulation of the atmosphere resulting from land-sea contrasts and orographic features. The land masses of Africa and Eurasia cover about 60% of the northeast quadrant of the globe whereas nearly 80% of the area is covered by water in the other three quadrants. Unlike the Atlantic and Pacific Oceans, the Indian Ocean is landlocked to the north by the Asian continent. The geographic setting gives rise to extreme thermal contrast between the land and the sea in the summer and in the winter, which is the crucial factor in the development of monsoon circulations in this region.

The mountain systems in this region play an important role in the generation and maintenance of the south Asian summer monsoon. The important features include the Himalayas and Tibetan plateau to the north, the Western Ghats on the Indian Peninsula, and the relatively flat Gangetic valley. The sharp gradient at the southern edge of the Tibetan plateau inherently makes numerical simulation for this region difficult.

Our study is concerned with the numerical simulation of monsoon depressions that frequently occur during the summer monsoon season. Monsoon depressions usually form over the warm Bay of Bengal and move morthwestward inland, bringing heavy precipitation to the northern Indian peninsula. These depressions can produce strong winds and weather phenomena in the northern Indian Ocean and the northern Arabian sea. It is hoped that sucessful numerical simulations of these depressions can lead to a better understanding of the relevant physical processes causing their genesis, intensification, decay, and interactions with larger scale circulation in this region. Such knowledge will eventually lead to better regional weather forecasts.

## 2.2 MODIFICATION OF THE MESOSCALE MODEL

Due to the high mountains and their proximity to the model lateral boundary it is nearly impossible to maintain a zero net mass inflow, which is one of the essential requirements of the model, within the domain shown in Figure 2.1. Thus ten grid points were added to each of the east and west lateral boundaries. The surface elevations of these grid points are linearly interpolated in the x-direction so that the elevations are uniformly zero at the outermost grid points. Gradually increased kinematic viscosity coefficients are applied to these additional grid points to serve as sponge boundaries. Because the prevailing large scale winds are predominately easterlies or westerlies, no additional grid points are needed along the north and south boundaries. However,

increased viscosity coefficients are applied there too. There are a total of 71 x 31 horizontal grid points and five sigma layers in the vertical, with $1^{\circ}$ horizontal resolution.

## 2.3 PRELIMINARY RESULTS

An idealized zonally mean field similar to that observed is used as the basic flow field (Fig. 2.2). The mean zonal flow includes westerlies at low levels with maximum speed of $\sim 7$ m $s^{-1}$ at $13^{\circ}$ and easterlies at high levels with a jet of more than 25 m $s^{-1}$ at low latitudes (Krishnamurti, 1971). In geostrophic balance with the mean flow, the temperature field has a 10 K north-south gradient in the midtroposphere.

The perturbations which initiate the monsoon depression are introduced to the model as prescribed heating pertinent to a cloud cluster. Saha et al (1981) found that more than 75% of monsoon depressions that occur in the Bay of Bengal can be traced by surface pressure tendency back to typhoons or tropical depressions in the Pacific Ocean. The remnants of these tropical disturbances, posing as cloud clusters, can redevelop once they move over the very warm Bay of Bengal. Earlier attempts were made to initiate monsoon depressions in our model by prescribing pressure tendency patterns. These attempts failed to generate strong enough perturbations in the momentum field, obviously due to the unfavorable mass-momentum adjustments on the scale of monsoon depressions. The prescribed heating currently applied produces suitable response in

the momentum field. The prescribed heating in the preliminary test presented next is kept stationary for 24 h. The heating in the model after 24 h is determined by the cumulus parameterization scheme.

Fig 2.3 shows the surface ($\sigma$ = 0.925) flow pattern at 48 h, when the center of the depression has just moved inland. The initial westerly jet at $\sim 13^{\circ}$ is enhanced over the Indian peninsula, and is turning into a southwesterly. It forms a trough in the Bay of Bengal, which supplies ample water vapor into the depression. There is a directional wind shear north of the depression caused by the gradient of the topography on the southern edge of the Tibetan plateau. The maximum wind shear near the depression center is $\sim 25$ m $s^{-1}$, in agreement with the observed strength. The depression moves west-northwest, against the surface westerlies, also in agreement with observations (Sikka, 1978).

It appears there are two major air streams into the depression. One extends from the westerly jet, and the other over the western Gangetic valley extends northwestward from the depression center. This suggests that the depression has frontal structure. Besides the depression center, there are two areas with heavy precipitation. One area is along the windslopes along the west coast of the Indian Peninsula between 7-17° latitude. The heavy and concentrated precipitation there is due to the lifting and frictional effects of the western Ghats. Heavy rainfall during the summer monsoon is often observed there (Ananthakrishnan, 1978). The second area of heavy precipitation outside the depression is associated with a strong convergence zone along the steep mountain slope at the southeast edge of the Tibetan plateau near 80°E and 27°N. In fact,

this "convergence" is fictitious. It arises because the lowest sigma layer follows the terrain in our model, in which vertical wind shears appear as horizontal convergence. This fictitious convergence causes an erroneous release of latent heat through the cumulus parameterization. Part of our future effort will focus on the improvement of Kuo's scheme in its application to sloped terrains.

Fig 2.4 shows the surface wind field at 72 h. The surface center has moved inland in a west-northwest direction with the maximum wind slightly decreased to 22 m $s^{-1}$. The decreased intensity is mainly due to increased surface friction and lack of moisture once the fetch from warm ocean becomes far. The Tibetan plateau has a great influence on the southly air flow originated from the Bay of Bengal and there appears to be a stagnant point at 90°E and 26°N. The surface winds are parallel to the slope west of this point.

## 2.4 SUMMARY

The initiation and movement of an idealized monsoon depression has been simulated with the NRL/SAI numerical model. The model domain covers an area from 50° - 100°E and 5° - 35°N. To improve the model, ten grid points have been added to the east and west lateral boundaries to smooth out the terrain and to serve as a sponge. There are five layers in the vertical, and the horizontal resolution is one degree.

An idealized zonal current pertinent to summer monsoon conditions is used as the basic current. Perturbations superposed on the mean current consist of a prescribed heating source appropriate to a propagating cloud cluster. Simulated surface wind fields at 48 and 72 h are presented and discussed. The simulation reproduces many observed phenomena associated with monsoon depressions. But Kuo's cumulus parameterization is found to give unrealistic heating near mountain slopes where vertical wind shear exist. Its application in the model in such regions needs further modification.

# CHAPTER 3. THE INTERACTIONS BETWEEN TWO TROPICAL CYCLONES

## 3.1 BACKGROUND

When two tropical cyclones are present simultaneously in the same region, it is often observed that they move around each other cyclonically. The phenomenon was first mentioned in Fujiwhara (1921), in which a mathematical approach was undertaken where the typhoons were represented by solid rotating vortices. Haurwitz (1951), examined several tropical cyclone pairs by introducing the concept of the center of mass around which the two tropical cyclones rotate at a rate given by the gradient winds. Liu and Wang (1966), studied some recent cases in the Pacific Ocean. They found that the two interacting tropical cyclones are not always attracted to each other, especially when there is a large shear in the basic flow.

Because most tropical cyclone pairs occur over the open ocean where data is sparse, researchers had to work with no more than conventional isobaric analyses with no details of flow fields. These analyses may contain factors such as shears in the basic flow and changes in the intensity that can obscure the true interactions. Our effort was to simulate this phenomenon with a numerical model and to isolate the Fujiwhara effects in an environment with no large scale flow.

## 3.2 THE NUMERICAL MODEL

The numerical model is identical to the one in Chang and Madala (1980), except for the parameterization of the latent heating. Here, a prescribed heating is used. The heating rate is defined as

$$\dot{Q}_o(r,\sigma) = \begin{cases} \dot{Q}_o \cos\left(\frac{\pi r}{R}\right) \cos\left[\frac{\pi(\sigma-0.5)}{0.45}\right], & \text{for } r \le R,\ 0.1 \le \sigma \le 0.9 \\ 0, & \text{otherwise} \end{cases} \tag{3.1}$$

where r is the distance between a grid point and the low pressure center, R = 300 km is the radius of the heating pattern, and $\dot{Q}_o$ is the maximum heating rate. Two values of $\dot{Q}_o$, 100 K day$^{-1}$ and 200 K day$^{-1}$, are used in various experiments to define the weak and strong tropical cyclone. The spatial distributions of the heating pattern are illustrated in Fig. 3.1. The heating pattern follows the low pressure centers which are determined by a linear interpolation of surface pressures.

The model has 51 x 51 horizontal grid points with seven sigma layers in the vertical. The horizontal resolution is 1/2°. The east-west boundaries are cyclic, and a sponge boundary condition is applied to the north and the south boundaries.

The heating prescribed by (3.1) generates a very realistic flow field for tropical cyclones. Figure 3.2 shows the radial distribution of the quasi-steady wind speeds at the 6th and the 7th model layers after 24 h of stationary heating with $\dot{Q}_o$ = 200 K day$^{-1}$. The wind speeds have a peak at r = 1° and decrease gradually outward without any noticeable

discontinuity at r=R. We note that by using the prescribed heating, we cannot simulate the effects of the interaction between the two storms on the cumulus convection in each individual storm, which in turn may alter the interactions by changing the storm's intensity. But these effects may be secondary and only important when the tropical cyclone pair are close. As a preliminary study, we opt to use the more economical prescribed heating to study the first order effects.

The two tropical cyclones are dynamically initialized by 24 h of stationary heating at two locations $\sim 10^{\circ}$ in longitude apart and at the same latitude. Fig 3.3 shows the surface pressure field at 24 h in a case where strong heating ($\dot{Q}_o$ = 200 K day$^{-1}$) is applied at both locations. The southward displacement of the western storm (storm A) and the northward displacement of the eastern storm (storm B) indicate that their interaction has already caused the two storms to rotate cyclonically, in spite of the stationary heating. Note the heating is allowed to move, following the low pressure centers after the 24 h initialization period. All numerical experiments in our study are listed in Table 3.1.

TABLE 3.1

| EXP. | $\dot{Q}_o$ for storm A ($K\ day^{-1}$) | $\dot{Q}_o$ for storm B ($K\ day^{-1}$) | Coriolis Parameter ($s^{-1}$) |
|---|---|---|---|
| 1. | 200 | 200 | $f=4.37 \times 10^{-5}$ |
| 2. | 100 | 100 | " |
| 3. | 100 | 200 | " |
| 4. | 200 | 200 | real f |
| 5. | 100 | 200 | " |
| 6. | 200 | 100 | " |
| 7. | 200 | - | " |

3.3.1 ON f-PLANE

Exps. 1-3 are intergrated with a constant f. Therefore the orientation has no meaning and the results are independant of the absolute initial positions of the storms. Figure 3.4 shows the trajectories of the storm centers in Exp. 1, in which two model tropical cyclones are of the same strength. The trajectories show that the two storms rotate about each other in a cyclonic fashion before the coalescence after 96 h. The two trajectories are symmetric about a center of mass, which happens to be the

center of the model domain. Superimposed on the symmetric rotation there is a convergence of the two tropical cyclones. The distance between the two storms decrease from ∿1024 km at 24 h to ∿612 km at 96 h. The symmetry remains until after 96 h when the two heating patterns overlap and one single large area of low pressure is formed.

Exp. 2 is identical to Exp. 1 except that the heating rate is halved. The cyclonic trajectories (Fig. 3.5) are still remarkably symmetric about the center of mass. Because of the weaker heating, two identifiable centers still exist at 120 h when they are only ∿100 km apart. We take note again that important feedbacks between cumulus convection and the storm pair's interaction may have been lost due to the prescribed heating in our model.

The speeds at which the two tropical cyclones in Exps. 1 and 2 rotate around and approach each other are shown in Fig. 3.6. The tangential velocity of the cyclonic rotation in Exp. 1 increases from ∿3 m $s^{-1}$ at 24-36 h to well over 6 m $s^{-1}$ after 72 h as the separation between the two tropical cyclones becomes small. The rotation speeds in Exp. 2 are about 1 m $s^{-1}$ slower than those in Exp. 1. Haurwitz (1951), pointed out that the rotation rate is proportional to the combined circulation strength of the two tropical cyclones, which was defined as the mass flow between two subjectively selected isobars. Using the average

maximum winds in our model as a measure of the combined strength, we found the relationship between the rotation rate and the strength of the interacting tropical cyclones postulated by Haurwitz (1951) to be neither clear nor well-defined. It is surprising, however, that the rate of convergence is independent of the combined strength as indicated by the radial velocities in Fig. 3.6.

Fig. 3.7 shows the trajectories of the two storm centers in Exp. 3, in which the maximum heating rate in storm A is only half that of storm B. We see that the two storms still rotate about each other cyclonically and that they still move toward each other. However, the trajectories are asymmetric and the weaker storm A moves much faster than the stronger storm B in a way similar to that of a binary celestial system in which the two bodies have different masses. This type of interaction has been observed between Typhoons Flossie and Grace (1950) (Liu and Wang 1966). The center of rotation is not stationary. Instead, it moves within a small area defined by the lines connecting the two storm centers at different times.

Results in Exps. 1-3 demonstrate that on an f-plane the interactions between two tropical cyclones consist of a cyclonic rotation, attraction, and eventual coalescence.

In order to examine the airflow fields associated with the interaction, we transform the model 500 mb wind fields in Exp. 1 onto a polar grid with respect to the center of the model domain. We now define the azimuthal mean velocity as

$$\bar{\underset{\sim}{V}} = \left[\bar{v}_r, \bar{v}_t, \bar{v}_z\right] = \frac{1}{2\pi}\int \left[v_r, v_t, v_z\right] d\theta \qquad (3.2)$$

where $v_r$, $v_t$, $v_z$ are radial, tangential and vertical velocities on the polar grid, and $\theta$ is the azimuthal angle. Fig. 3.8 shows the azimuthally mean vertical, tangential, and radial velocities at 24, 48, 72, and 96 h. It is interesting that the mean momentum fields relative to the center of domain shown here are very similar to those in intensifying tropical cyclones. For example, at 24 h there is a maximum mean tangential velocity of $\sim$4 m $s^{-1}$ at r $\sim$600 km and a minimum of $\sim$−2 m $s^{-1}$ at r $\sim$400 km reflecting the cyclonic wind fields about the two storm centers. The maximum tangential velocity gradually increases to $\sim$16 m $s^{-1}$ and moves toward the center to $\sim$350 km at 96 h. The maximum inflow also develops from 2 m $s^{-1}$ at r $\sim$600 km at 24 h to $\sim$4 m $s^{-1}$ at r $\sim$350 km at 96 h. The evolution of the mean vertical velocity is also similar to that of an intensifying and contracting tropical cyclone.

The development of the azimuthal mean circulation can also be illustrated by comparing the kinetic energy (KE) of the mean velocity (KEM) and the KE of the eddy velocity (KEE), where

$$KEM = \iint 1/2 \left[\bar{v}_r, \bar{v}_t\right] \cdot \left[\bar{v}_r, \bar{v}_t\right] r \, dr \, d\theta ,$$

$$KEE = \iint 1/2 (v_r', v_t') \cdot (v_r', v_t') \, r \, dr \, d\theta , \qquad (3.3)$$

$$\text{where } (v_r', v_t') = (v_r, v_t) - \left[\bar{v}_r, \bar{v}_t\right].$$

As shown by Fig. 3.9, the KEE, which can mostly be attributed to the circulations around the two centers, reaches a quasi-steady state after 36 h. Meanwhile the KEM, representing the strength of the mean circulation as depicted by Fig. 3.8 around the center of rotation, steadily increases until the coalescence of the two tropical cyclones. The ratio of KEE/KEM decreases from ∿3 at 24 h to less than 1 at 96 h.

These analyses suggest that a mean circulation relative to the center of rotation develops due to the interaction of two tropical cyclones. This mean circulation includes tangential and radial components resembling those associated with tropical cyclones. The cyclonic and convergent movements of two interacting tropical cyclones are believed to be caused by the advective effects of the "mean" circulation.

### 3.3.2 THE EFFECTS OF VARIATIONS OF THE CORIOLIS PARAMETER

Exps. 4-7 were carried out with variable Coriolis parameter,

which can produce a northwestward drift of tropical cyclone in the northern hemisphere (Adem, 1956; Madala and Piascek, 1975; Chang and Madala 1982; Holland, 1982). The velocity of the drift depends on the latitude and on the cyclone's strength. To examine the free drift of a single tropical cyclone in our model, we carried out Exp. 7. As shown by trajectory C in Fig. 3.10, the model tropical cyclone has an initial northward movement, but changes toward the northwest after 36 h. The 0-72 h mean drift velocity is 1.18 m $s^{-1}$ toward the west and 1.37 m $s^{-1}$ toward the north. The center at 72 h is $\sim 6^{\circ}$ to the west and $\sim 6.5^{\circ}$ to the north of the initial position.

The latitudinal variations of the Coriolis parameter have a very pronounced effect on the trajectories of the two interacting tropical cyclones. The trajectories of the two tropical cyclones with equal strength in Exp. 4 is shown in Fig. 3.10. Instead of rotating around the + point as in Exp. 1, the tropical cyclone to the west (storm A) moves toward the southeast then quickly turns toward the northeast, while the tropical cyclone to the east (storm B) rapidly moves northwestward and rotates cyclonically with respect to storm A. The two storms eventually coalesce at 87 h, with storm B having traveled a much larger distance from its initial position than storm A. We have computed the trajectories A and B relative to storm C (Exp. 7) in an attempt to remove the beta-drift——although the removal is imcomplete in that storm C, while having the same strength,

cannot be at the same latitude and therefore the same drift speed simultaneously with both storms A and B. The resultant relative trajectories (not shown) are very similar to those in Exp. 1 (Fig. 3.3). We therefore conclude that the asymmetric trajectories exhibited by two interacting tropical cyclones on a real f surface consist of the symmetric rotation found on an f-plane and a beta drift toward the northwest.

Exp. 5 is to compared with Exp. 3, where storm A is weaker than storm B. The trajectories of the storm centers in Exp. 5 (Fig. 3.11) again appear very different from those in Exp. 3. The stronger storm B shows more noticable northwest drift than in Exp. 3. The weaker storm A rotates cyclonically toward the southeast at a much reduced rate and with a smaller radius, apparently due to the counteracting beta drift.

Most interesting is Exp. 6, in which storm A is stronger than storm B. From 24 to 72 h, the weaker storm B moves cyclonically relative to storm A. In the meantime storm A moves slowly toward the southeast nearly perpendicular to and away from storm B. We believe that this is due to a combination of the interaction and the stronger beta drift of storm A. The trajectories take a strange turn after 72 h because the two storms start to influence each other through the cyclic east-west boundaries.

It can be concluded that the latitudinal variation of the Coriolis parameter has profound impact on the trajectories of two interacting storms. The northwest drift caused by the beta effect greatly distorts the symmetric, cyclonic rotation found on an f-plane. The differential beta drift also can make two interacting tropical cyclones move apart if the storm to the west is stronger.

## 3.4 SUMMARY

The interaction between two tropical cyclones (the Fujiwhara effect) is simulated and studied with the NRL/SAI mesoscale numerical model. Included in the model are parameterizations of boundary layer and latent heating with presribed spatial distribution moving with the low pressure center. The model contains 51 x 51 x 7 grid points with 1/2 degree horizontal resolution. The east-west boundary conditions are cyclic and the north-south boundaries are sponge. The two tropical cyclones are dynamically initialized at the same latitude by a 24 h stationary heating at two centers $10^{\circ}$ in longitude apart.

Results show that on an f-plane with no mean wind, the movements of the two cyclones consist of a mutual cyclonic rotation and attraction. The spiral-like paths of the two cyclones of equal (different) strength are symmetric (asymmetric) relative to the "center of mass" of the two cyclones. The rate of rotation

is approximately proportional to the combined strength of the two tropical cyclones while the rate of convergence is not. The two tropical cyclones eventually coalesce.

Further analyses show that the cyclonic rotation and the mutual attraction of two interacting cyclones are related to the development of a "mean" circulation about the center of mass, similar in itself to a weak tropical cyclone, while the "eddy" kinetic energy about the centers of the two interacting tropical cyclones remains relatively invariant.

When the latitudinal variation of the Coriolis parameter is included in the model, the movements of two interacting tropical cyclones are complex. The trajectories of two equally strong tropical cyclones include a symmetric cyclonic rotation with a northwestward beta drift. The rate of their mutual rotation seems to be unaffected by the variable Coriolis parameter. The location of the eventual coalescence is $\sim 6^{\circ}$ to the northwest of the initial center of mass. If the tropical storm to the west is stronger than the one to the east, we found that they move away from each other because the differential beta drifts overcome the mutual attraction.

# CHAPTER 4 EASTERLY WAVES

## 4.1 BACKGROUND

The existence of westward traveling wave disturbances in the easterly tropical belt has been established since the studies by Riehl (1945) and Palmer (1952). Later studies yielded a more dynamically and thermodynamically consistent picture of these easterly waves (see Reed, et al, 1977 for review). It is known that most tropical cyclones have their origins in the easterly waves (Gray, 1979). Our current study is concerned with a numerical simulation of the transformation of easterly waves into incipient tropical cyclones.

## 4.2 THE EASTERLY WAVE MODEL

The NRL/SAI mesoscale numerical model was modified to facilitate the simulation of easterly waves. For this simulation there were 51 x 31 horizontal grid points with one degree resolution and five sigma layers in the vertical. The east-west lateral boundaries are cyclic and the second derivatives of thermodynamic variables normal to the boundary vanish at the north-south boundaries. Kuo's (1975) cumulus parameterization scheme and Chang's (1981) boundary layer parameterization scheme were employed in the model.

In order to simplify our initial attempt, the initial basic easterly current is set uniformly at $\sim$5 m $s^{-1}$. The Coriolis parameter is constant throughout the model domain and equals $5 \times 10^{-5}$ $s^{-1}$. Observational and theoretical studies on easterly waves have suggested that barotropic (mainly latitudinal wind shear) instability and beta effects are important for the intensification of tropical disturbances. We temporarily leave these factors out for simplicity.

## 4.3 PRELIMINARY RESULTS

The initial perturbation is introduced by a prescribed 6 h stationary heating with similar spatial distribution as that in Section 2 but with a lower maximum heating rate of 20 K $day^{-1}$. Fig. 4.1 shows the model eastwest cross-section of latitudinal components of the wind velocity (v), vertical velocity (w), and relative humidity (RH) at 48 h. In the v field, the maximum perturbations occur at the lowest layer ($\sigma$ = 0.975) and $\sigma$ = 0.2. The amplitude is $\sim$6 m $s^{-1}$ with cyclonic vorticity at low levels and anticyclonic vorticity at higher levels. Compared with a phase III GATE composite (Fig. 4.2, from Reed et al, 1977), the model simulated latitudinal wind components are very realistic in the vertical structure and the amplitude, including the westward tilt of the zero dividing line of south/north components. The observed maximum perturbation

occurs at ∿700 mb instead of at low levels, while the maximum vorticity is in the lowest level in our model. This is related to the undesirably strong convective heating between 700 mb and the surface in our model.

The simulated vertical motion field is understandably noisier than the observed composite. In composite analyses, small scale perturbations such as gravity waves caused by moist convection shown here in our model, are largely smoothed out. However, the maximum upward velocity in our model is ∿24 mb $h^{-1}$, four times stronger than the observed. We recall that there are no barotropic nor baroclinic instabilities in our basic flow field. The model tropical disturbance is mainly sustained by the convection, which tends to produce strong vertical motions in spite of the rather realistic v components. The model results can be improved by including barotropic instability in the basic easterly flows.

The observed location of the maximum upward motion is about 1/8-1/4 wavelength ahead of the surface trough line, whereas in the model results the displacement is smaller. This decrepancy is conjectured to be the result of the absence of the beta effect in the model.

The model RH field agrees well with the observations. There is a deep moistened troposphere behind the trough with RH>70% up to ~400 mb. The midtroposphere in front of the trough is slightly dryer than the environment.

## 4.4 SUMMARY

Preliminary results of an attempt to simulate easterly waves are presented. In this attempt, no initial barotropic nor baroclinic instability in the basic flow are included. The results show that a tropical disturbance is realistically simulated with good structure in the horizontal wind field and the RH field. The results are very encouraging and suggest that the beta-effect and latitudinally sheared basic easterlies be included in future attempts.

## REFERENCE


Adem, J., 1956: A series solution for the barotropic vorticity equation and its application in the study of atmospheric vortices. Tellus, 8, 364-372.

Ananthakrishnan, 1978: Some aspect of the monsoon circulation and monsoon rainfall. Monsoon Dynamics P. 1209, Birkhauser Verlag.

Chang, S. W., 1981: Test of a planetary boundary layer parameterization based on a generalized similarity theory in tropical cyclone models. Mon. Wea. Rev., 109, 843-853.

Chang, S. W., and R. V. Madala, 1980: Numerical simulation of the influence of sea surface temperatures on tranlating tropical cyclones. J. Atmos. Sci., 36, 2617-2630.

Fujiwhara, S., 1921: The natural tendency towards symmetry of motion and its application as a principle in meteorology. Quart J. Roy. Meteor. Soc., 47, 287-293.

Gray, W. M. 1979: Hurricanes: their formation, structure, and likely role in the tropical circulation. Meteorology Over the Tropical Oceans, Royal Meteor. Soc., Billing and Sons Limited, Guildford, London 155-218.

Haurwitz, B., 1951: The motion of binary tropical cyclones. Arch. Meteor. Geoph. Biokl., (A)4, 73-86.

Holland, G. J., 1982: Tropical cyclone motion: environmental interaction plus a beta effect Atmospheric Science Paper 348, Department of Meteorology, Colorado State University, ISSN 0067-0340.

Krishnamurti T. N., 1971: Observational study of the tropical upper troposphere motion field during the northern hemisphere summer. J. Appl. Meteor., 10, 1066-1096.

Kuo, H. L., 1974: Further studies of the parameterization of the influence of cumulus convection on large scale flow. J. Atmos. Sci., 31, 1232-1240.

Liu, D. L. and S. T. Wang, 1965: Case study of interactions of Pacific Ocean Typhoons. Quart J. Weather Forecasting and Analysis (in chinese).

Madala, R. V. and S. A. Piacsek, 1975: Numerical simulation of asymmetric hurricanes on a β-plane with vertical shear. Tellus, 27, 453-468.

Palmer, C. P., 1952: Tropical Meteorology. Quart J. Roy. Meteor., 78, 126-163.

Reed, R. J., D. C. Norquist, and E. E. Recker, 1977: The structure and properties of Africa wave disturbances as observed during phase III of GATE. Mon. Wea. Rev., 105, 317-333.

Riehl, H. 1945: Waves in the easterlies and the polar front in the tropics. Misc. Report No. 17, Dept. of Meteorology, University of Chicago, 79 pp.

Saha, K., F. Sanders, and J. Shukla, 1981: Westward propagating predecessors of monsoon depressions. Mon. Wea. Rev., 109, 330-343.

Sikka, D. R., 1978: Some aspects of the life history, structure and movement of monsoon depressions. Monsoon Dynamics, P. 1501, Birkhauser Verlag.

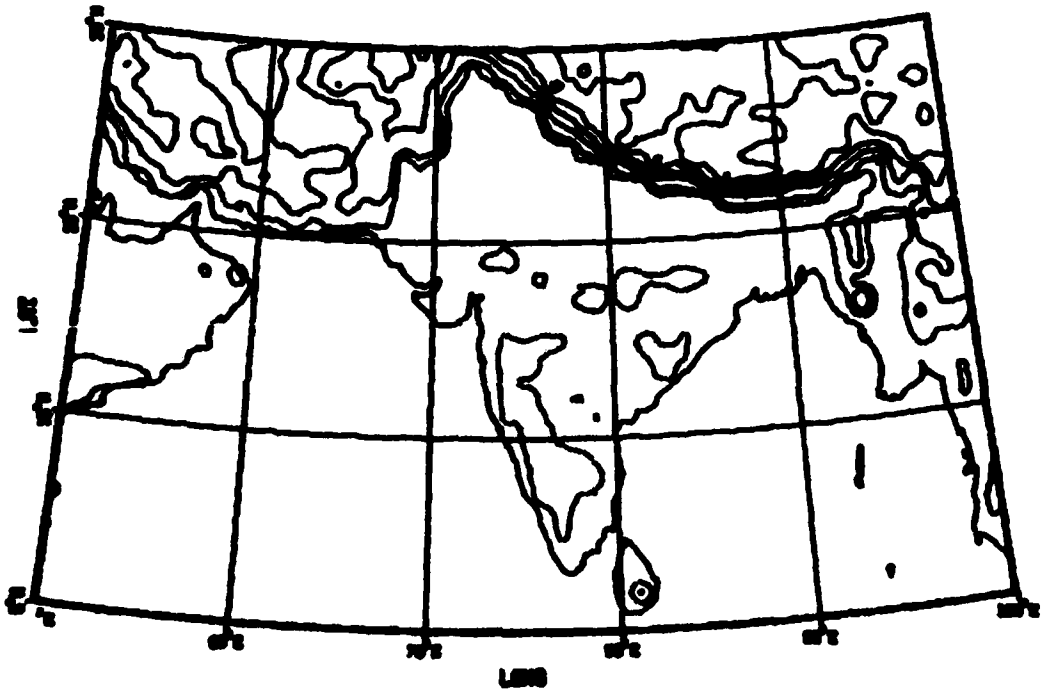

Fig 2.1 The domain of the monsoon depression model. Contours are surface elevations of 500 (dashed), 1000, 2000, 3000 ... etc.,m.

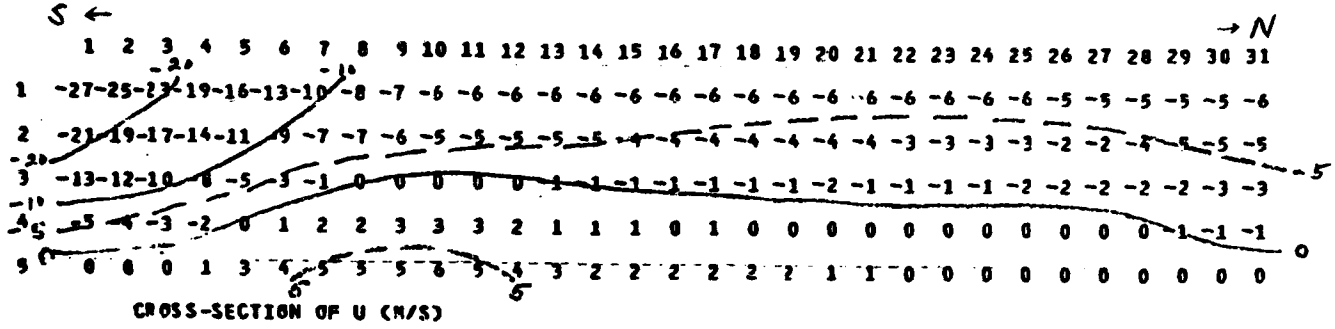


Fig 2.2 The north-south cross-section shows the zonal basic current for the monsoon depression experiment.

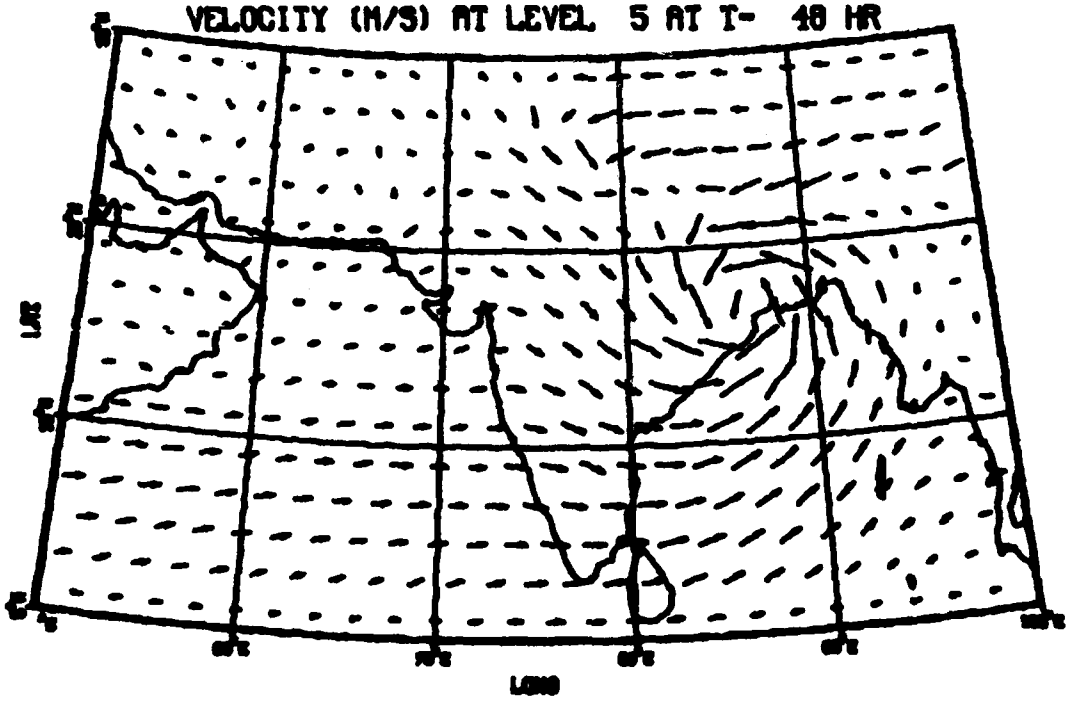


Fig 2.3 Surface wind vectors for monsoon depression experiment at 48 h.

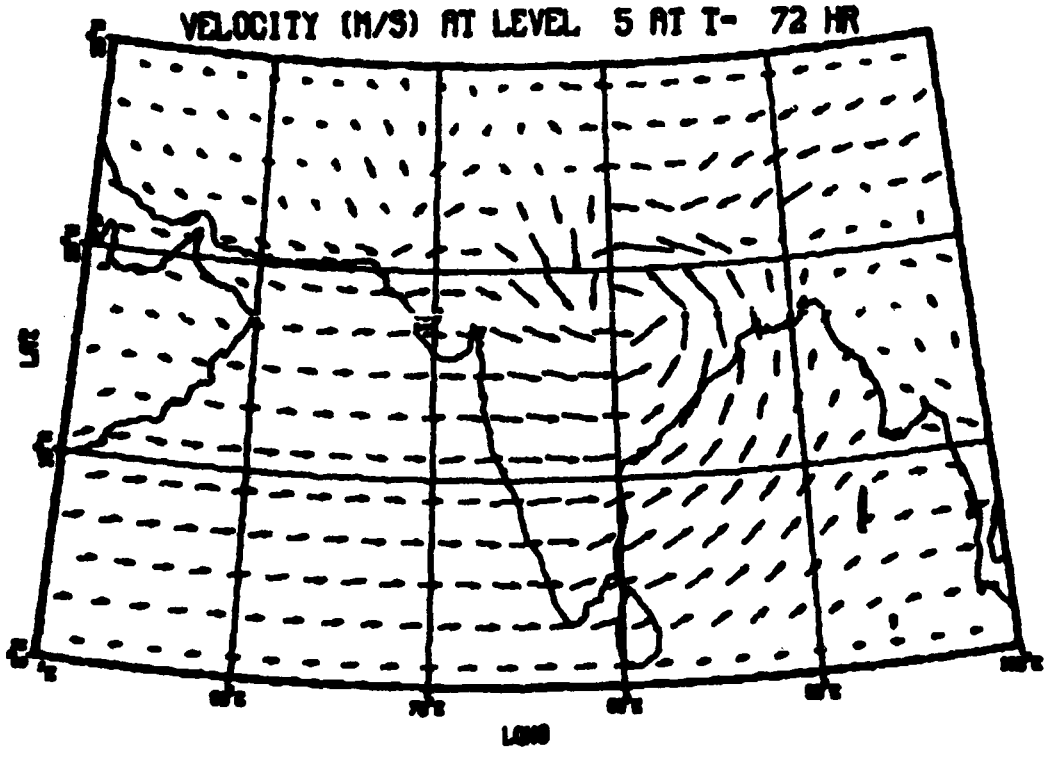


Fig 2.4 As in Fig. 2.3 except for at 72 h.

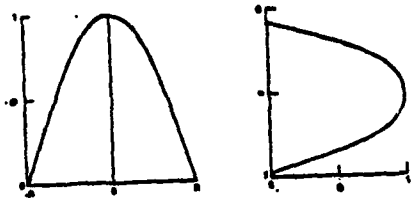

Fig 3.1 The horizontal and vertical distribution of the prescribed heating pattern used in the Fujiwhara effect experiments.

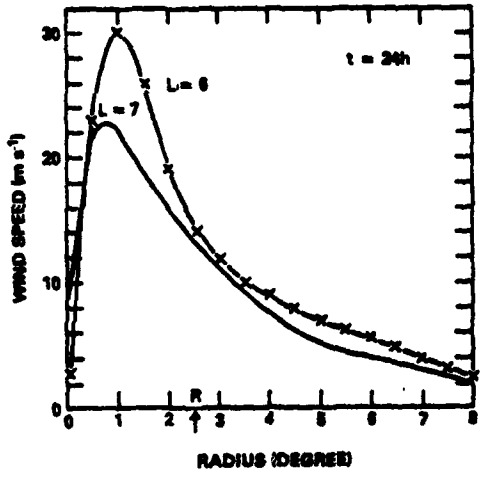


Fig 3.2 The radial distribution of the quasi-steady wind speeds generated by the stationary prescribed heating.

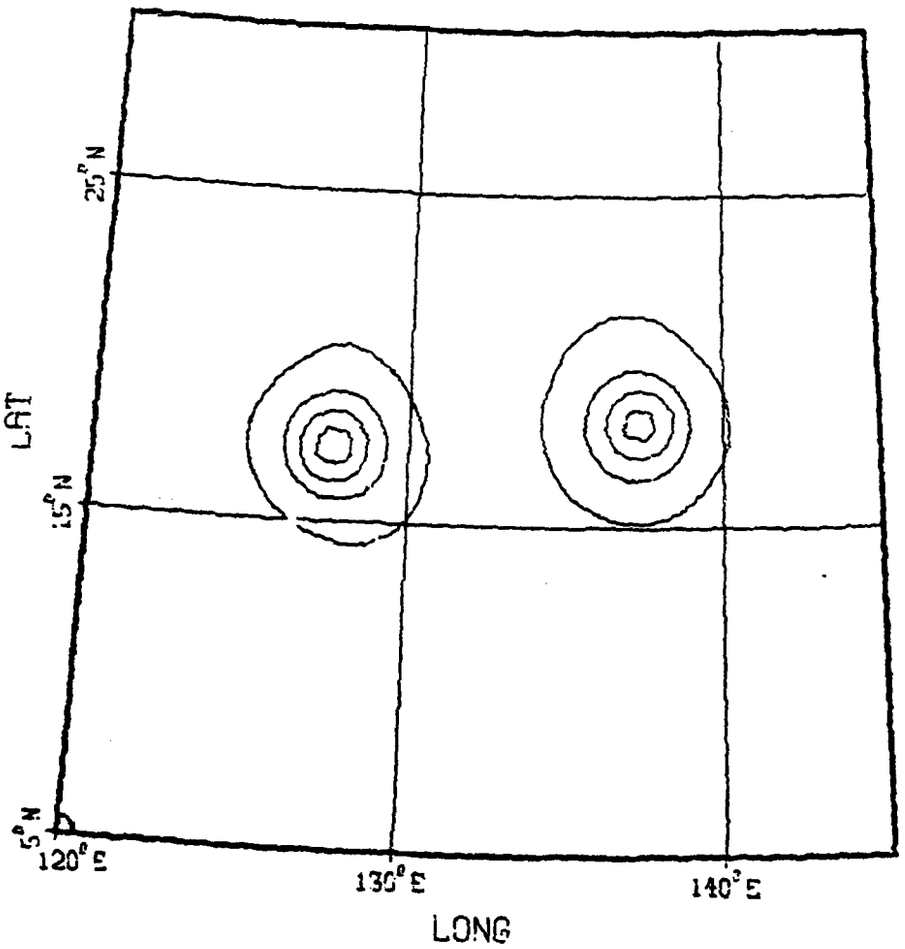


Fig 3.3 The surface pressure field at 24 h for Exp. 1. Contour intervals are 4 mb, the outermost closed isobars are 1008 mb.

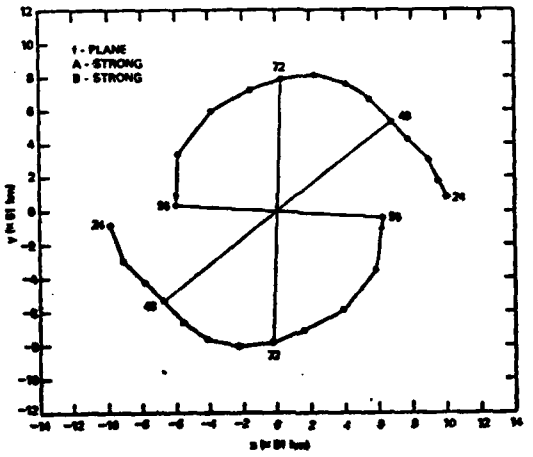


Fig 3.4 The trajectories of storm centers in Exp. 1. Numbers on the curve denote times in hour.

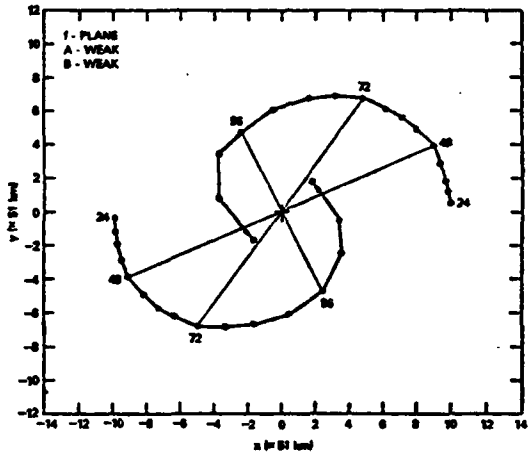


Fig 3.5 As in Fig. 3.4, except for Exp. 2.

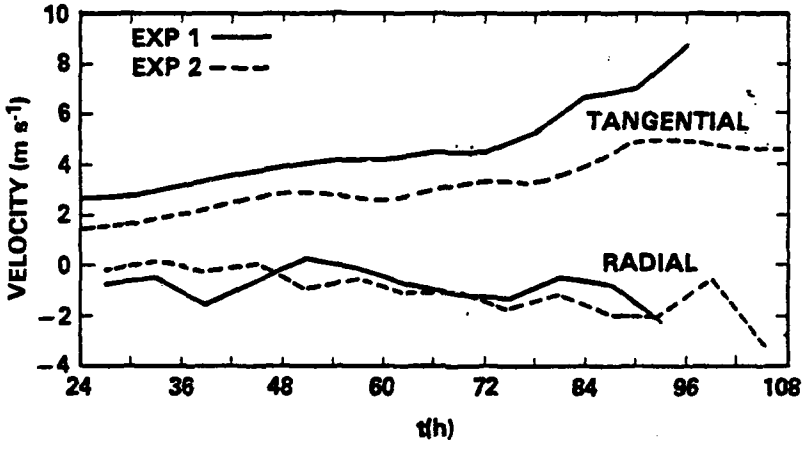


Fig 3.6 The tangential and radial speeds of the centers of the two interacting tropical cyclones relative to their center of mass in Exps. 1 and 2.

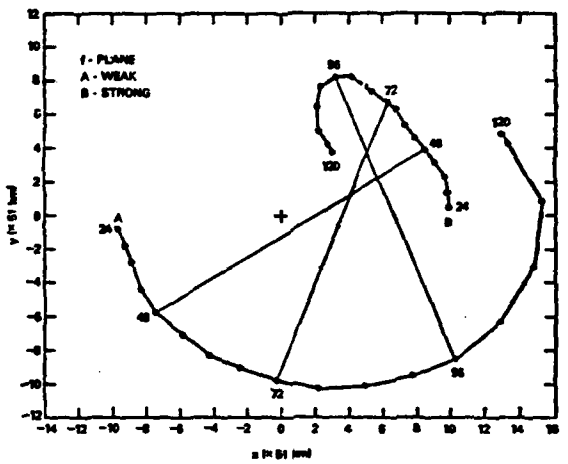


Fig 3.7 As in Fig 3.4 except for Exp. 3.

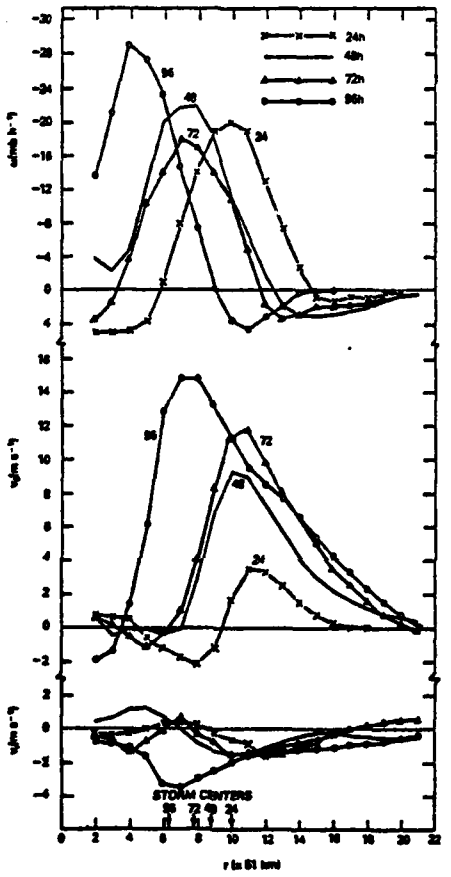


Fig 3.8 The azimuthal mean radial ($V_r$), tangential ($V_\theta$), and vertical velocities of the wind field relative to the center of mass in Exp. 1.

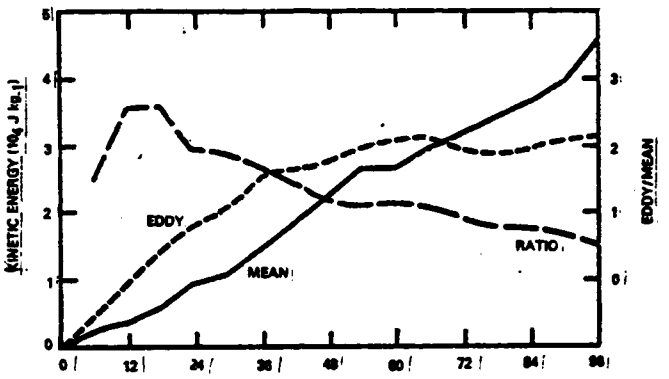


Fig. 3.9 The development of the kinetic energy of the "mean" flow (solid) relative to the center of mass and the kinetic energy of the "eddy" associated with the two storm centers (dashed) in Exp. 1.

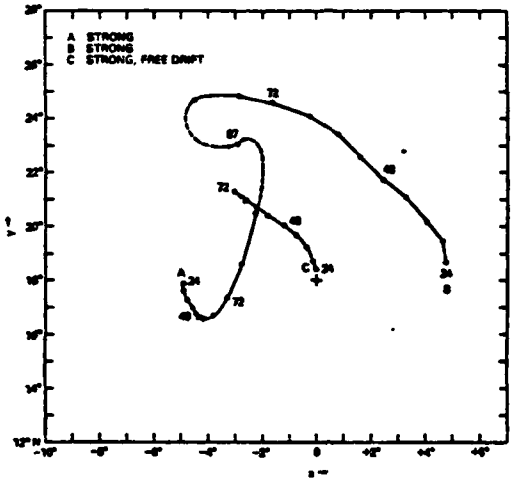


Fig 3.10 The trajectories of the free drifting storm in Exp. 7 (curve C) and of two interacting storms in Exp. 4 (curves A and B).

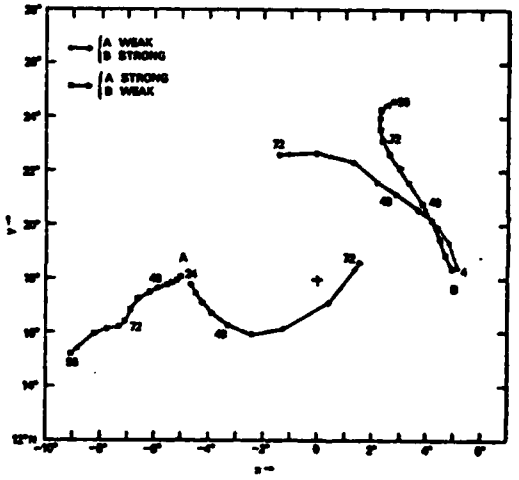


Fig 3.11 As in Fig 3.10, except for Exps. 5 (solid lines with dots) and 6 (solid lines with squares).

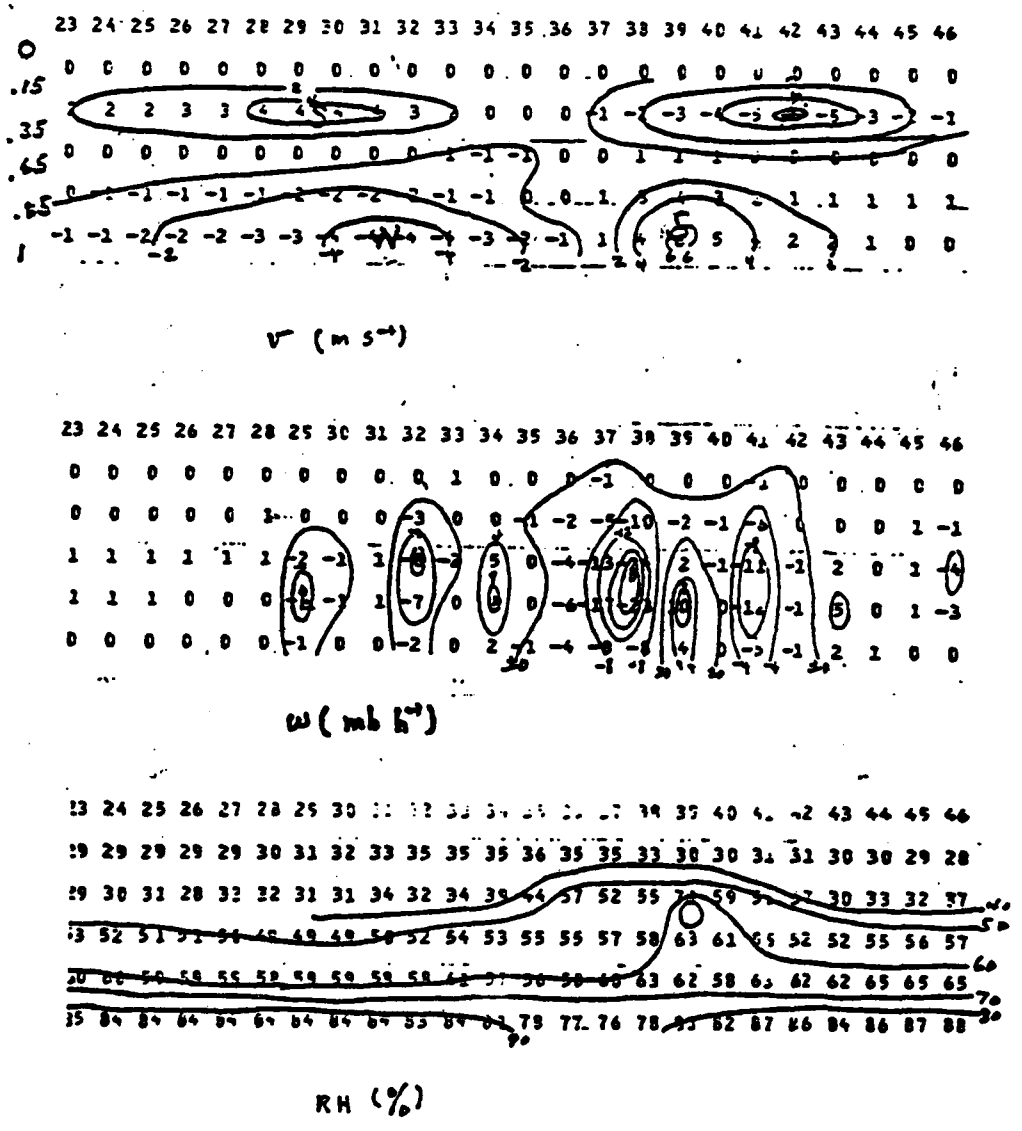


Fig 4.1 East(right)-west(left) cross-section of the easterly wave model showing (a) the latitudinal component of wind velocities in m $s^{-1}$ (upper panel) (b) the vertical velocities in w $h^{-1}$ (middle panel), and (c) the relative humidities in % (lower panel) associated with a model easterly wave at 48 h.

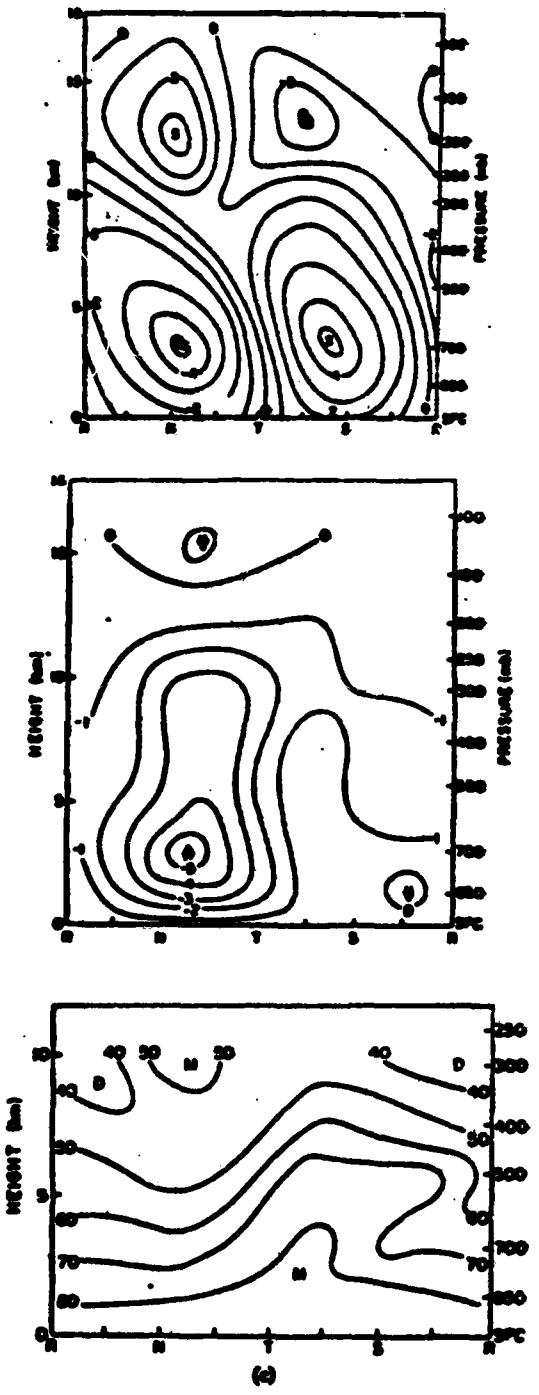

Fig 4.2 As in Fig. 4.1 except for composite analyses of GATE easterly waves (Reed et al, 1977).

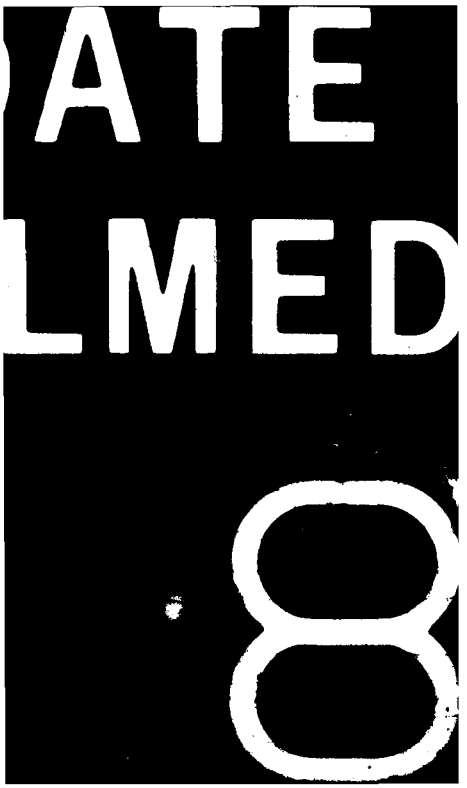
ATE
LMED
8